# Fabrication of Na$_{0.4}$MnO$_2$ Microrods for Room-Temperature Oxidation of Sulfurous Gases

Nishesh Kumar Gupta, Srungarpu N. Achary, Herlys Viltres, Jiyeol Bae,* and Kwang Soo Kim*

Cite This: *ACS Omega* 2022, 7, 37774−37781

Read Online

ACCESS | Metrics & More | Article Recommendations | Supporting Information

**ABSTRACT:** Phase pure Na$_{0.4}$MnO$_2$ microrods crystallized in the orthorhombic symmetry were fabricated for the wet oxidation of H$_2$S and SO$_2$ gases at room temperature. The material was found highly effective for the mineralization of low concentrations of acidic gases. The material was fully regenerable after soaking in a basic H$_2$O$_2$ solution.
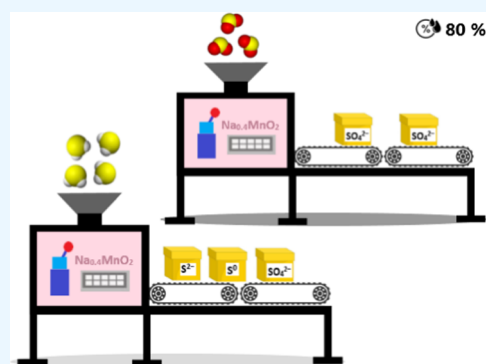
## 1. INTRODUCTION

Sodium transition metalates are notable materials for developing cathodes of Na-ion rechargeable batteries.[1,2] The redox reactions mediated by the transition metal ions during their application as cathode materials[3,4] could be exploited for multielectron catalytic reactions. The strong redox property of transition metal ions (especially 3d metals) in Na metalates has found application as an electrocatalyst for water splitting.[5,6] Na$_x$MnO$_2$ has been studied for low-temperature water splitting in a reversible thermochemical cycle[7] and as a heterogeneous catalyst for the oxidative cleavage of 1,2-diols to aldehydes/ketones.[8] Moreover, when coupled with $\alpha$-MnO$_2$, the composite could catalyze the ammoxidation−Pinner tandem reaction.[9]

Among many other applications possible for Na$_x$MnO$_2$ like radionuclide sequestration,[10,11] these materials could find use in the oxidation of acidic gases, which is largely unexplored in the literature. These inexpensive and nontoxic materials have strong basic sites, which could be effective in the remediation of acidic gases like hydrogen sulfide (H$_2$S) and sulfur dioxide (SO$_2$). These gases are highly toxic to living beings even at a very low concentration of 1−5 ppm and fatal at a higher concentration of 100−500 ppm.[12,13] Moreover, these gases are considered precursors for acid rain formation and particulate matter, known to cause human casualties and loss of vegetation.[14,15] The removal of these contaminants at a low concentration from their sources is challenging and requires expensive techniques for clean-up.[16,17]

Here, we have explored the use of an inexpensive and readily available alkali ceramic material for the wet-oxidative removal of low concentrates of acidic gases in ambient conditions. The material of choice, i.e., pure Na$_{0.4}$MnO$_2$, was synthesized in a three-step method using Mn(II) acetate and Na(I) acetate as precursor salts. The synthesized material was studied for the room-temperature oxidative removal of H$_2$S and SO$_2$ gases at low concentrations. Besides understanding the underlying mechanisms for the capture of sulfurous gases, we have reported an economic, environmentally friendly, and easy method for the regeneration of spent oxide. This study has presented a detailed application of the phase pure Na$_{0.4}$MnO$_2$ material for room-temperature removal of toxic sulfurous gases.

## 2. EXPERIMENTAL SECTION

**2.1. Chemicals.** Manganese(II) acetate tetrahydrate (Mn-(CH$_3$COO)$_2$·4H$_2$O), sodium acetate trihydrate (CH$_3$COONa·3H$_2$O), H$_2$O$_2$ solution (28−30 vol %), and NaOH solution (5 mol L$^{-1}$) were purchased from Samchun Pure Chemicals, Korea. Highly pure H$_2$S (500 ppm) and SO$_2$ (100 ppm) gases in N$_2$ gas were procured from Union Gas, Korea. All of the chemicals were of analytical grade and used without any further purification.

**2.2. Synthesis of Na$_x$MnO$_2$.** Exactly 25.0 g of Mn acetate and 6.8 g of Na acetate were dissolved in a minimum volume of deionized water. The solution was placed in a hot air oven at
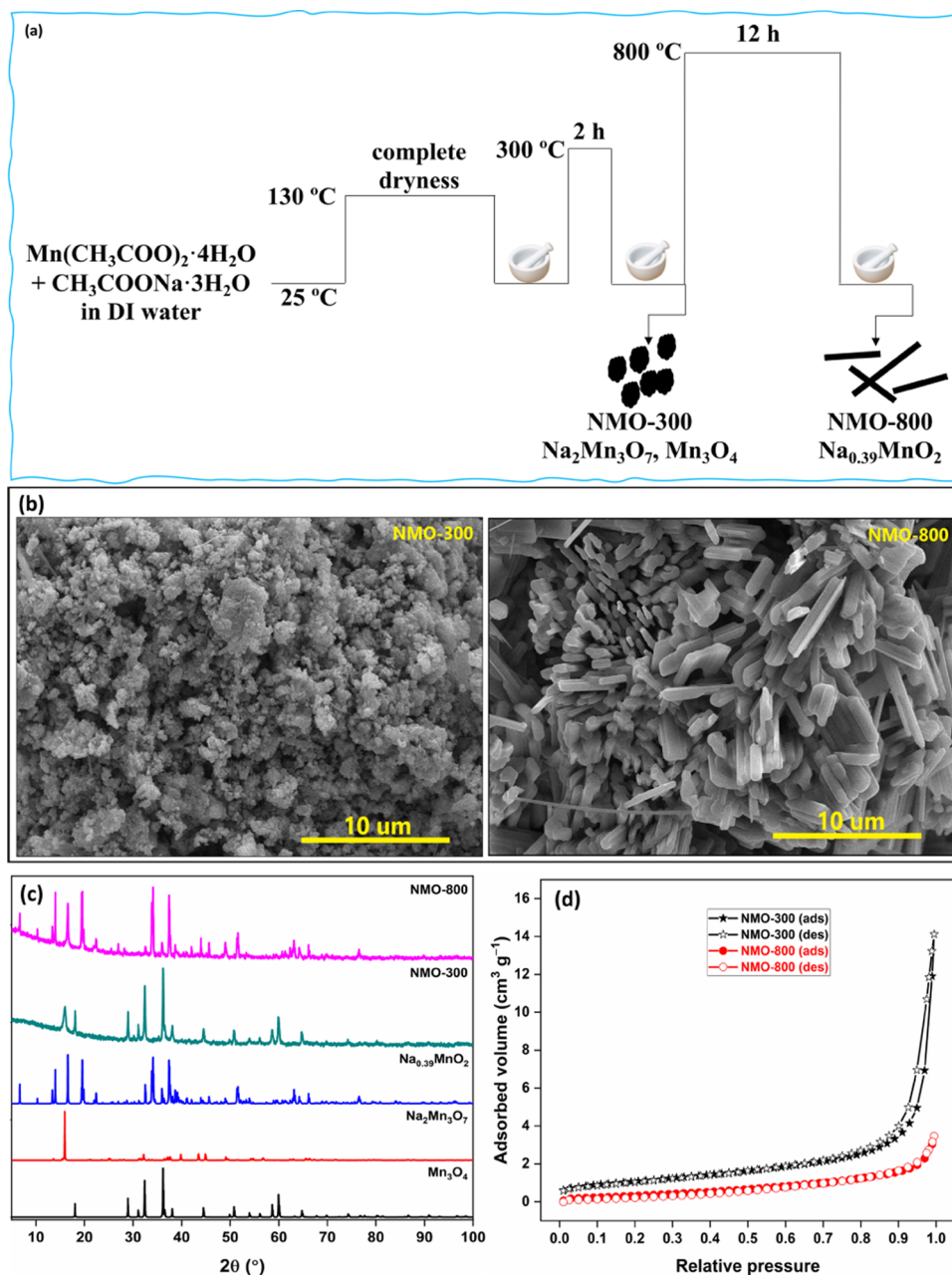
**Figure 1.** (a) Synthesis scheme, (b) SEM micrographs, (c) PXRD patterns, and (d) N$_2$ adsorption−desorption isotherms of NMO-300 and NMO-800.

130 °C till complete dryness. The dry solid mass was powdered thoroughly and introduced in a muffle furnace for calcination at 300 °C for 2 h. The formed solid mass was cooled to room temperature and powdered again. The product formed was named NMO-300. Half of the NMO-300 sample was calcined again at 800 °C for 12 h in the muffle furnace to yield NMO-800.

**2.3. Analytical Instruments.** The oxide morphology was probed through field emission scanning electron microscopy (FE-SEM, Hitachi S-4300, Hitachi, Japan) and field emission transmission electron microscopy (FE-TEM, JEM-2010F, JEOL Ltd., Japan). Elemental mapping was conducted using energy-dispersive X-ray spectroscopy (EDAX, X-Max 80T, Oxford Instruments, U.K.) in TEM mode. The X-ray diffraction patterns were recorded at 298 °C at 2θ between 5 and 100° on an Ultima IV (Rigaku, Japan) X-ray

diffractometer with Cu Kα radiation (λ = 1.5406 Å) and a Ni filter. Fourier transform infrared (FTIR) spectra were collected over a Cary670 FTIR spectrometer (Agilent Technologies). The specific surface area and porosity of samples were determined by analyzing the standard N$_2$ adsorption−desorption isotherm at −196 °C using a Gemini 2360 series (Micromeritics) instrument after degassing at 150 °C for 8 h. X-ray photoelectron spectroscopy (XPS, Nexsa X-Ray Photoelectron Spectrometer System, Thermo Scientific, U.K.) was used to determine the chemical states of the elements in the prepared oxides. A monochromatic Al Kα X-ray source was used with a fixed pressure of $4.8 \times 10^{-9}$ mbar. Spectra were charge corrected to the main line of the C 1s spectrum (aromatic carbon) set to 284.7 eV. Spectra were analyzed using CasaXPS software (version 2.3.14) with GL($p$) = Gaussian/Lorentzian product formula, where the mixing is
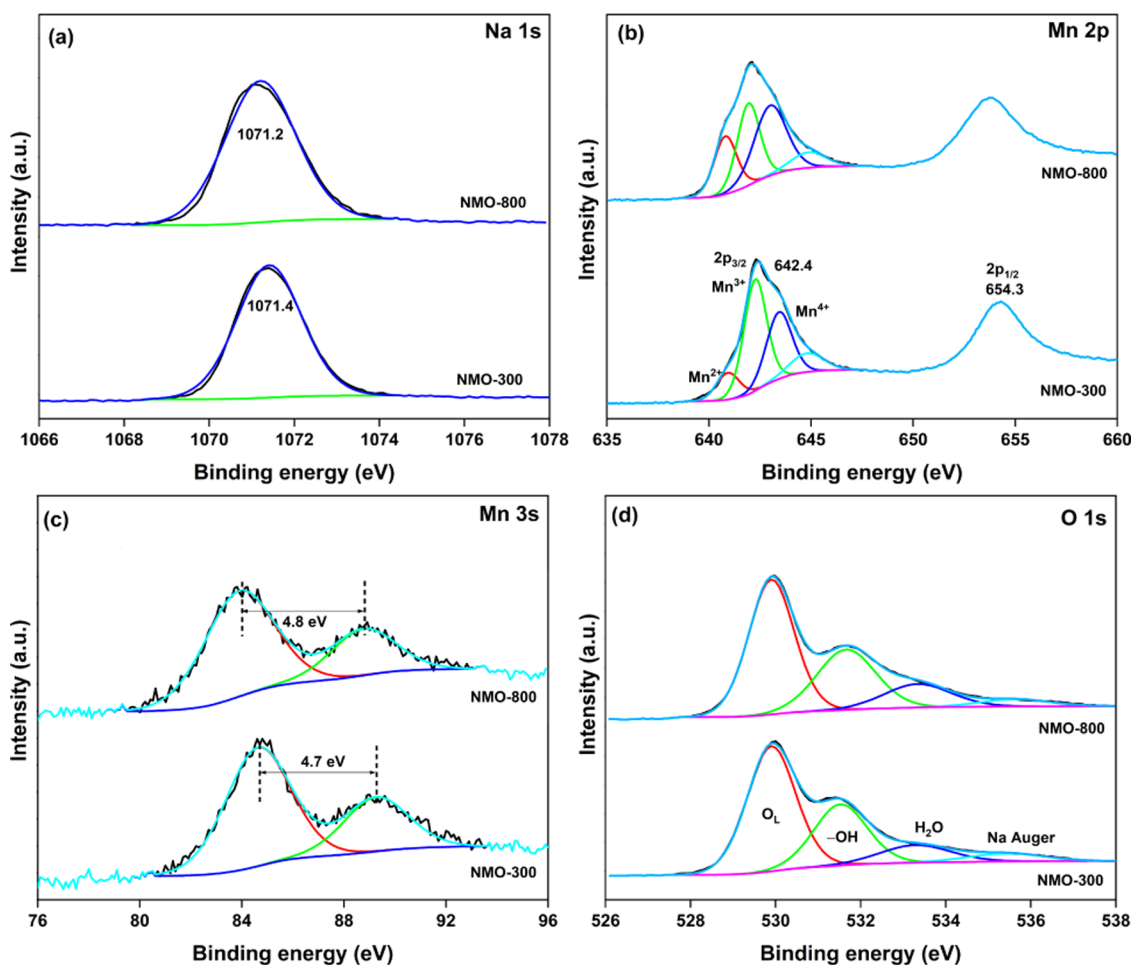
**Figure 2.** HRXPS (a) Na 1s, (b) Mn 2p, (c) Mn 3s, and (d) O 1s spectra of NMO-300 and NMO-800.

determined by $m = p/100$, GL(100) is a pure Lorentzian, and GL(0) is a pure Gaussian. We used GL(30).

**2.4. Experimental Protocol.** A 0.3 g of the adsorbent was placed in a Pyrex tube between glass wool and a gas flow of 0.2 L min$^{-1}$ was maintained. The samples were fully saturated with moisture by blowing moist air (80% relative humidity) at 25 °C for 8 min through the adsorbent bed from a humidifier. The H$_2$S concentration in the outflow gas was analyzed by an H$_2$S gas analyzer (GSR-310, Sensoronic, Korea). The SO$_2$ concentration in the effluent gas was analyzed using a GASTIGER 6000 SO$_2$ analyzer. The adsorption capacity ($q$, mg g$^{-1}$) at the breakthrough point (20% of the input gas) was calculated by the following equation

$$q = \frac{C_0 Q}{m} \int_0^{t_b} \left(1 - \frac{C}{C_0}\right) dt \tag{1}$$

where $C_0$ is the initial concentration, $Q$ is the flow rate, $m$ is the mass of oxide (g), and $t_b$ is the breakthrough time.

The spent adsorbent was regenerated by soaking it in a binary solution (10 mL) of 0.25 mol L$^{-1}$ NaOH and 0.49 mol L$^{-1}$ H$_2$O$_2$ for 6 h. The material was dried and studied for the next adsorption cycle. The same solution was reused for the subsequent regeneration cycles. A mass loss during the regeneration process was expected and because of this, a normalized time was adopted to calculate the adsorption capacity.

## 3. RESULTS AND DISCUSSION

The precursors were dissolved in a minimal volume of water under ultrasonication, and then the water was evaporated at 130 °C. The dried powder was precalcined at 300 °C for acetate decomposition. The material was labeled NMO-300. NMO-300 was further calcined at 800 °C to achieve the desired product (NMO-800, Figure 1a). Microscopic analyses showed irregularly shaped nanoparticles for NMO-300 and a network of smooth microrods for NMO-800 (Figures 1b and S1).[18] The XRD patterns were analyzed by the Rietveld refinement method using earlier reported structural details (Figure S2). In NMO-300, we have identified triclinic Na$_2$Mn$_3$O$_7$ (space group $P\bar{1}$, lattice constants: $a = 6.604$ Å, $b = 6.851$ Å, $c = 7.527$ Å, $\alpha = 106.29°$, $\beta = 106.63°$, $\gamma = 111.65°$)[19] and tetragonal Mn$_3$O$_4$ (space group: $I41/amd$, lattice constants: $a = 5.752$ Å, $c = 9.455$ Å).[20] The NMO-800 sample has highly crystalline microrods of Na$_{0.39}$MnO$_2$ crystallized in an orthorhombic lattice with the space group Pbnm ($a = 9.080$ Å, $b = 26.461$ Å, $c = 2.824$ Å; Figure 1c).[21] The N$_2$ adsorption−desorption isotherms resemble Type III isotherms exhibited by nonporous or macroporous materials (Figure 1d).[22] The NMO-300 sample possessed a surface area of 3.85 m$^2$ g$^{-1}$, which dropped to 1.45 m$^2$ g$^{-1}$ for NMO-800 due to increased particle size (Table S1).[23]

The HRXPS Na 1s spectra of NMO samples have a peak at 1071.2−1071.4 eV for Na$^+$ ions (Figure 2a).[24] The HRXPS Mn spectrum of NMO-300 has two peaks at 642.4 and 654.3

eV for $2p_{3/2}$ and $2p_{1/2}$ doublets, respectively. The Mn $2p_{3/2}$ spectrum was deconvoluted into three contributions at 640.9, 642.3, and 643.4 eV for $Mn^{2+}$ (12.7%), $Mn^{3+}$ (52.2%), and $Mn^{4+}$ (35.1%) ions, respectively.[25] The presence of $Mn^{2+}$ was associated with $Mn_3O_4$. Also, the presence of $Mn^{2+}$ could be linked to the $Na_2Mn_3O_7$ phase. Hakim et al. confirmed the presence of $Mn^{2+}$ ions on the surface of $Na_2Mn_3O_7$, which remained absent in the bulk phase of the material.[26] The Mn $2p_{3/2}$ peak of NMO-800 has all three curves at 640.8, 641.9, and 643.0 eV with 24.4, 34.1, and 41.5% contributions, respectively (Figure 2b). In previous studies on $Na_{0.4}MnO_2$, only +3 and +4 oxidation states for Mn have been reported.[24,27] However, it is likely possible to have all three Mn oxidation states in $Na_xMnO_2$-type materials as observed in our previous work.[28] The Mn 3s spectra of NMO samples have an energy separation of 4.7−4.8 eV, indicating the dominance of +3 and +4 oxidation states in the samples (Figure 2c).[29] The HRXPS O 1s spectrum of NMO-300 deconvoluted into four curves centered at 529.9 (57.6%), 531.5 (30.8%), 532.3 (11.6%), and 535.4 eV for lattice oxygen ($O_L$), surface-bound hydroxyl groups (−OH), adsorbed $H_2O$,[30] and Na Auger,[31] respectively (Tables S3−S5). For NMO-800, these four contributions are present with a slightly higher proportion of −OH groups and adsorbed $H_2O$ (Figure 2d).

NMO-300 and NMO-800 have been studied for $H_2S$ and $SO_2$ adsorption in 80% relative humidity with initial gas concentrations of 500 and 100 ppm, respectively. The dynamic breakthrough studies were performed with a breakthrough point at 20% of the influent concentration (Figure 3). The $H_2S$ adsorption capacity of 2.81 mmol $g^{-1}$ for NMO-300 improved to 3.59 mmol $g^{-1}$ for NMO-800 (Figure 3a). The $SO_2$ adsorption capacities of 0.55 and 0.61 mmol $g^{-1}$ were achieved for NMO-300 and NMO-800, respectively (Figure 3b). The adsorption of $H_2S$ or $SO_2$ could be possible through direct oxidation by $O_L$ or by interacting with the −OH groups.[28,32,33] Here, we have observed similar proportions of these oxygen species in both samples. Moreover, the surface area of NMO-300 was higher than that of NMO-800. So, it seems peculiar to have a higher gas uptake capacity for NMO-800. However, NMO-300 has a significant proportion of the $Mn_3O_4$ phase, which is considered a poor adsorbent for room-temperature acidic gas capture.[34] We also observed higher basicity of NMO-800 when soaked in water, which could be responsible for its higher acidic gas uptake (Figure S3). Thus, we expected NMO-800 to be a better adsorbent for sulfurous gas capture owing to more favorable acid−base reactions. The regenerability of NMO-800 was studied for three adsorption−regeneration cycles. The spent oxide was regenerated using an inexpensive and nontoxic $NaOH−H_2O_2$ solution simply by soaking at room temperature. The idea behind adopting this method was to eliminate the dependency on the thermal regeneration method, which is energy-intensive and produces secondary pollutants ($SO_x$).[35] The regeneration method was highly effective and showed an improvement in $H_2S$ uptake from 5.29 mmol $g^{-1}$ in the first cycle to 7.46 mmol $g^{-1}$ in the third cycle (Figure 3a inset). Likewise, the $SO_2$ uptake capacity of 0.87 mmol $g^{-1}$ in the first cycle reached 1.03 mmol $g^{-1}$ in the third cycle (Figure 3b inset). Such a positive trend during the regeneration process could be because of decreasing oxide mass in the subsequent cycles (Figure S4). But it is confirmed that NMO-800 could maintain a high gas uptake capacity using the developed regeneration method.
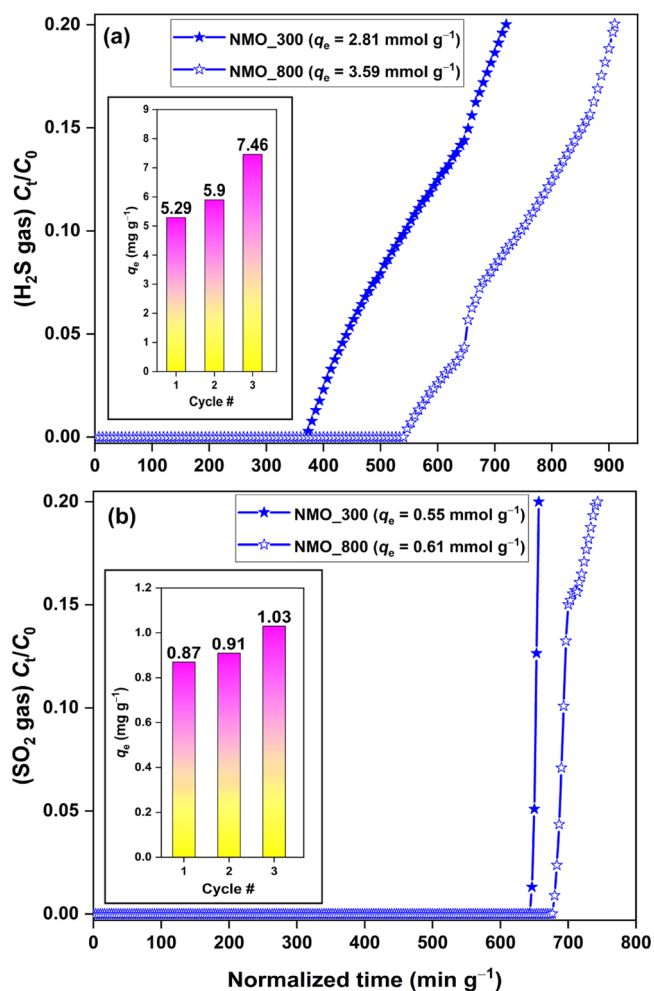


**Figure 3.** (a) $H_2S$ and (b) $SO_2$ breakthrough curves for wet NMO-800 samples. Experimental conditions: flow rate = 0.2 L $min^{-1}$, mass = 0.3 g. Inset: regeneration capacity of NMO-800. Conditions: flow rate = 0.2 L $min^{-1}$, mass = 0.15 g.

First, the water-exposed NMO-800 after drying was analyzed to probe any structural−property change in the material. The XRD pattern showed no crystallographic change with an insignificant variation in the lattice constants (Figure S5 and Table S2). However, the surface area dropped to 0.97 $m^2$ $g^{-1}$, which may not have played any major role in the process, as the reactions are expected to occur on the material surface (Figure S6). Even XPS analyses confirmed that there was a minuscule variation in the surface −OH density and Mn oxidation state distribution (Figure 4). The only observable parameter that changed was the increase in the surface basicity of NMO-800, which is expected to be of prime importance in surface reactions of acidic gases (Figure S3).[36] Thus, we have concluded that the adsorbed water may have not altered the NMO-800 properties to a greater extent, but it helped in promoting $H_2S/SO_2$ dissolution and dissociation on the basic NMO-800 surface.[32,37]

The PXRD analyses of gas-exposed NMO-800 have all of the peaks intact with minor changes in the lattice constants. However, some additional peaks were probably related to the $Na_2Mn(SO_4)_2 \cdot xH_2O$ phase.[38] The inference is based on the presence of sulfate as an end-product in both $H_2S$- and $SO_2$-exposed samples (Figure S5). The XPS survey confirmed S 2p peaks in 160−170 eV for gas-exposed samples (Figure 4a).
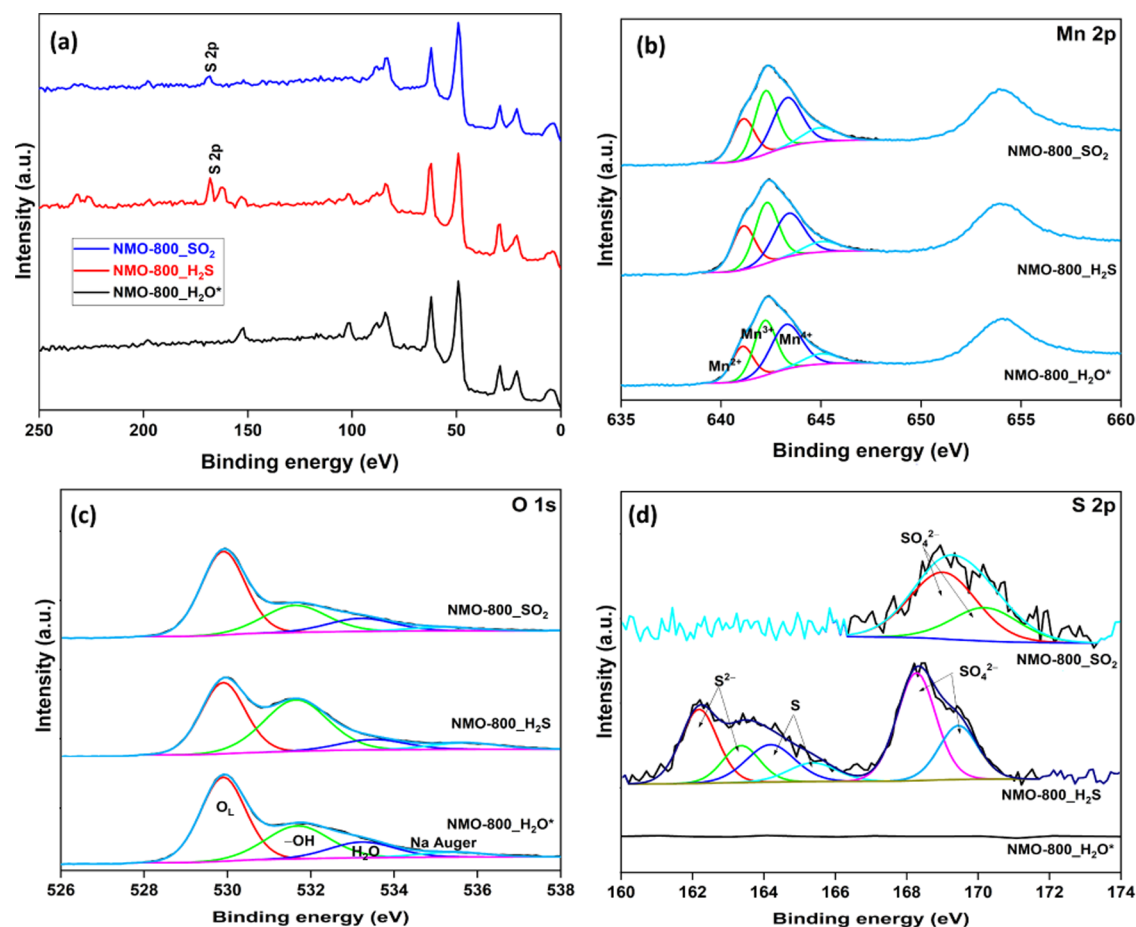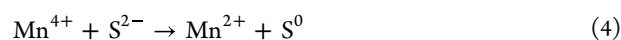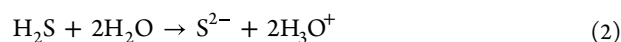
**Figure 4.** (a) XPS survey and HRXPS (b) Mn 2p, (c) O 1s, and (d) S 2p of water adsorbed−desorbed and gas-exposed NMO-800.

The Mn 2p spectra of NMO-800_H₂S and NMO-800_SO₂ have higher concentrations of $Mn^{2+}$ and $Mn^{3+}$ ions at the expense of $Mn^{4+}$ ions. The oxidation of H₂S or SO₂ is accompanied by the reduction of $Mn^{4+}$ ions to $Mn^{3+}/Mn^{2+}$ ions,[33,37] which is expected in the present case. However, the variation in the $Mn^{4+}/(Mn^{2+} + Mn^{3+})$ ratio is not large for these samples, which could be associated with the oxidation of +2 and +3 back to +4 ions by molecular O₂.[28,37] Thus, it was conclusive that $Mn^{4+}/Mn^{3+}/Mn^{2+}$ redox cycles drove the gas oxidation reactions over the NMO-800 surface (Figure 4b). A significant drop in the $O_L$ component in NMO-800_H₂S was largely associated with the replacement of $O^{2-}$ with $S^{2-}$ ions (Figure 4c). More information from O 1s spectra could not be extracted due to the mixing of the S−O component (from $SO_4^{2-}$) in −OH due to similar binding energy at 531.8 eV.[39] The formation of $SO_4^{2-}$ (as H₂SO₄) is associated with the drop in the surface basicity, which was observed for NMO-800 as the pH value fell from 11.5 (for NMO-800_H₂O*) to 11.1 and 10.0 for H₂S-, and SO₂-exposed NMO-800, respectively. This was a strong indication of more H₂SO₄ formation during the SO₂ capture process and not H₂S capture (Figure S3). More validation on the formed sulfur species of the oxidation process was deduced from the S 2p spectra. The S 2p spectrum of NMO-800_H₂S has three $2p_{3/2}–2p_{1/2}$ doublets. The $2p_{3/2}$ peaks at 162.2, 164.2, and 168.3 eV were associated with the formation of $S^{2-}$ (31.2%), $S^0$ (20.8%), and $SO_4^{2-}$ species (48.0%, Table S6).[40] These oxidative species have been previously reported for room-temperature H₂S oxidation over $NaMn_xO_y$[28] or $Co_3O_4$.[41]

H₂S gas adsorbed and dissociated in the surface water film to form $S^{2-}$ ions (eq 2). Moreover, H₂S molecules could react with the −OH groups to yield $HS^-$ ions (eq 3).[42] These $S^{2-}$ ions were oxidized to $S^0$ via $Mn^{4+}$ ions with the formation of $Mn^{3+}/Mn^{2+}$ ions (eqs 4 and 5). These $Mn^{2+}/Mn^{3+}$ ions were reverted to $Mn^{4+}$ ions by adsorbed molecular O₂ (eqs 6 and 7). Moreover, $S^{2-}$ species was oxidized by molecular O₂ to form $SO_3^{2-}$ species (eq 8), which readily oxidized to $SO_4^{2-}$ ions (eq 9). In the entire adsorption−oxidation reaction, adsorbed molecular O₂ played a significant role in running the $Mn^{2+}/Mn^{3+}/Mn^{4+}$ redox cycles and conversion of H₂S gas. NMO-800_SO₂ has only one doublet with the S $2p_{3/2}$ peak at 169.0 eV for $SO_4^{2-}$ species.[33] This behavior is in line with the previously reported work on SO₂ interaction with $Li_2MnO_3$, where SO₂ oxidized to $SO_4^{2-}$ species (Figure 4d).[43,44] Similar results are available for SO₂ oxidation over $Na−MnO_x$ in moist conditions.[33] SO₂ gas molecules reacted with the adsorbed water to form $HSO_3^-$ ions (eq 10). Moreover, SO₂ interacted with the lattice oxygen to form $SO_3^{2-}$ ions (eq 11). These $SO_3^{2-}$ ions readily oxidized on the oxide surface by the action of molecular O₂ to yield $SO_4^{2-}$ ions (eq 9). Even SO₂ molecules could reactively interact with the surface −OH groups to yield $HSO_3^-$ ions (eq 12).[45]
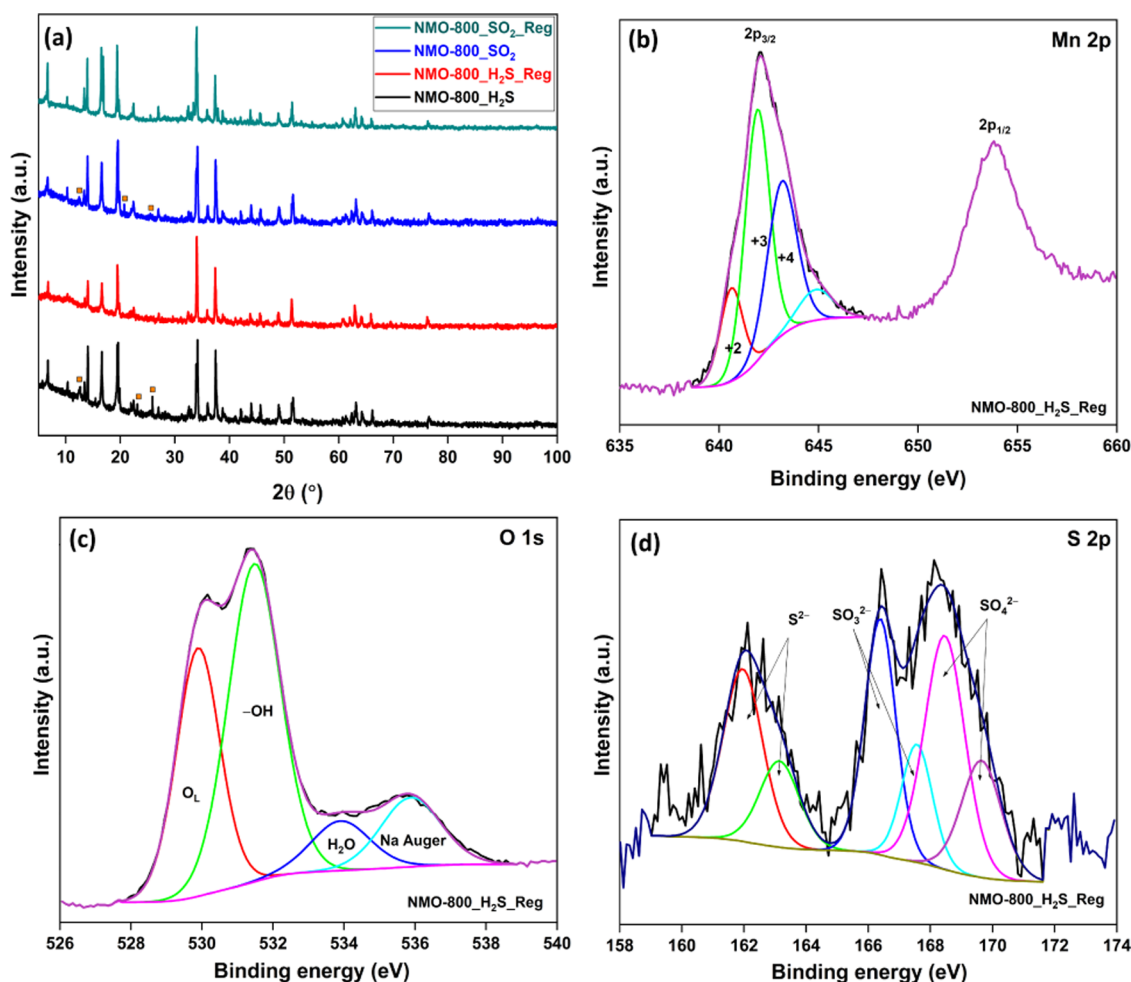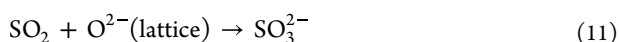
$$H_2S + 2H_2O \rightarrow S^{2-} + 2H_3O^+ \tag{2}$$

$$H_2S + -OH \rightarrow -OH_2^+ + HS^- \tag{3}$$
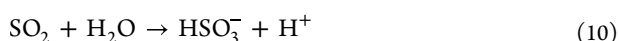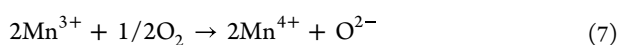
$$Mn^{4+} + S^{2-} \rightarrow Mn^{2+} + S^0 \tag{4}$$

**Figure 5.** (a) PXRD patterns and HRXPS (b) Mn 2p, (c) O 1s, and (d) S 2p of spent NMO-800 after regeneration.

$$2Mn^{4+} + S^{2-} \rightarrow 2Mn^{3+} + S^0 \qquad (5)$$

$$Mn^{2+} + 1/2O_2 \rightarrow Mn^{4+} + O^{2-} \qquad (6)$$

$$2Mn^{3+} + 1/2O_2 \rightarrow 2Mn^{4+} + O^{2-} \qquad (7)$$

$$S^{2-} + 3/2O_2 \rightarrow SO_3^{2-} \qquad (8)$$

$$SO_3^{2-} + 1/2O_2 \rightarrow SO_4^{2-} \qquad (9)$$

$$SO_2 + H_2O \rightarrow HSO_3^- + H^+ \qquad (10)$$

$$SO_2 + O^{2-}(lattice) \rightarrow SO_3^{2-} \qquad (11)$$

$$SO_2 + -OH \rightarrow -SO_3H \qquad (12)$$
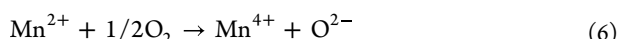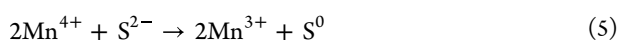
More information on the regeneration process was extracted from the experimental and spectroscopic analyses. First, the surface polarity of the regenerated samples was measured through conventional soaking of the samples in water. Aqueous pH values of 11.89 and 11.76 for regenerated NMO-800_H₂S and NMO-800_SO₂, respectively, showed that the regenerated samples were more basic compared to the pristine sample (Figure S3). This higher surface basicity is expected to improve the acidic gas capture capacity. On the structural front, these samples were characterized by PXRD (Figure 5a). The PXRD patterns of regenerated samples are like those of the spent or fresh samples, where $Na_{0.39}MnO_2$ (orthorhombic phase) was retained. However, there is a variation in intensity (peaks marked with orange-colored squares disappeared) and spacing between some peaks. This might be due to distortion induced by oxidation of Mn or orientation of grains of samples during the PXRD experiment.

The XPS analysis confirmed a significant drop in the sulfur content on the surface of the adsorbent surface after regeneration, i.e., from 4.0% in the spent sample to 1.5% in the regenerated sample (Table S7). This suggested the surface cleaning of the oxide during the regeneration process. The Mn 2p spectrum of NMO-800_H₂S_Reg showed a decreased proportion of $Mn^{2+}$ ions, which could favor the adsorption process based on eqs 6 and 7 (Figure 5b). The O 1s spectrum showed a hike in the −OH proportion, which could improve the H₂S dissociation over the oxide surface (Figure 5c). The S 2p spectrum confirmed significant variation in the sulfur species over the oxide surface (Figure 5d). The $S^0$ species was absent in the sample, which suggested complete washing of it during the regeneration process. Also, we observed a major drop in the proportion of $SO_4^{2-}$ species. Importantly, we confirmed a large concentration of $SO_3^{2-}$ species (a doublet with the $2p_{3/2}$ peak at 166.4 eV[46]), which was initially absent in the spent sample. The formation route for $SO_3^{2-}$ species could be the oxidation of $S^{2-}$ ions in the presence of $H_2O_2$.

## 4. CONCLUSIONS

In summary, we reported a novel method for the fabrication of phase pure $Na_{0.4}MnO_2$ microrods using a solid-state synthesis route. The fabricated Na−Mn oxide could effectively oxidize low concentrations of $H_2S$ and $SO_2$ gases at room temperature in the presence of moisture. We further demonstrated the complete regeneration of spent oxide using an affordable and environmentally benign basic $H_2O_2$ solution. The spectroscopic analyses confirmed the formation of oxidized sulfur byproducts for both $H_2S$ and $SO_2$ adsorption. Thus, for the first time, we reported the application of these cathodic materials for room-temperature oxidation of acidic sulfurous gases, which would broaden the scope of these materials beyond Na-ion batteries.

## ■ ASSOCIATED CONTENT

### ⓢ Supporting Information

The Supporting Information is available free of charge at https://pubs.acs.org/doi/10.1021/acsomega.2c04773.

> TEM images; Rietveld refinement plots of XRD data; pH of water after soaking of NMO samples; regenerability breakthrough curves; $N_2$ adsorption−desorption isotherm of NMO samples; and surface area and pore characteristics, lattice constants of crystals, and XPS fitting results for NMO samples (PDF)

## ■ AUTHOR INFORMATION

### Corresponding Authors

**Jiyeol Bae** − *Department of Environmental Research, University of Science and Technology (UST), Daejeon 34113, Korea; Department of Environmental Research, Korea Institute of Civil Engineering and Building Technology (KICT), Goyang 10223, Korea;* ⓞ orcid.org/0000-0001-6119-9349; Email: baejiyeol@kict.re.kr

**Kwang Soo Kim** − *Department of Environmental Research, University of Science and Technology (UST), Daejeon 34113, Korea; Department of Environmental Research, Korea Institute of Civil Engineering and Building Technology (KICT), Goyang 10223, Korea;* Email: kskim@kict.re.kr

### Authors

**Nishesh Kumar Gupta** − *Department of Environmental Research, University of Science and Technology (UST), Daejeon 34113, Korea; Department of Environmental Research, Korea Institute of Civil Engineering and Building Technology (KICT), Goyang 10223, Korea*

**Srungarpu N. Achary** − *Chemistry Division, Bhabha Atomic Research Centre, Mumbai 400085, India;* ⓞ orcid.org/0000-0002-2103-1063

**Herlys Viltres** − *School of Engineering Practice and Technology, McMaster University, West Hamilton, Ontario L8S 4L8, Canada*

Complete contact information is available at:
https://pubs.acs.org/10.1021/acsomega.2c04773

### Author Contributions

N.K.G. oversaw data curation, formal analysis, methodology, and writing of the original draft. N.K.G., S.N.A., H.V., and J.B. oversaw visualization and validation. K.S.K. and J.B. were responsible for funding acquisition, resources, and supervision.

### Notes

The authors declare no competing financial interest.

## ■ ACKNOWLEDGMENTS

## ■ REFERENCES

(1) Hwang, J.-Y.; Myung, S.-T.; Sun, Y.-K. Sodium-Ion Batteries: Present and Future. *Chem. Soc. Rev.* **2017**, *46*, 3529−3614.

(2) Nitta, N.; Wu, F.; Lee, J. T.; Yushin, G. Li-Ion Battery Materials: Present and Future. *Mater. Today* **2015**, *18*, 252−264.

(3) Zhan, C.; Wu, T.; Lu, J.; Amine, K. Dissolution, Migration, and Deposition of Transition Metal Ions in Li-Ion Batteries Exemplified by Mn-Based Cathodes − a Critical Review. *Energy Environ. Sci.* **2018**, *11*, 243−257.

(4) Stansby, J. H.; Sharma, N.; Goonetilleke, D. Probing the Charged State of Layered Positive Electrodes in Sodium-Ion Batteries: Reaction Pathways, Stability and Opportunities. *J. Mater. Chem. A* **2020**, *8*, 24833−24867.

(5) Li, B.; Wang, T.; Li, X.; Zheng, X.; Wu, X.; Zhu, J.; Xu, H. Activating P2-$Na_xCoO_2$ for Efficient Water Oxidation Catalysis via Controlled Chemical Oxidation. *Mater. Today Chem.* **2018**, *10*, 206−212.

(6) Song, S.; Wang, Y.; Davis, R. C.; Ren, Z.; Xiao, X.; Yang, G.; Wang, D.; Bao, J.; Zhang, Q.; Chen, S.; Ren, Z. Electrochemical Insight into $Na_xCoO_2$ for the Oxygen Evolution Reaction and the Oxygen Reduction Reaction. *Chem. Mater.* **2021**, *33*, 6299−6310.

(7) Xu, B.; Bhawe, Y.; Davis, M. E. Low-Temperature, Manganese Oxide-Based, Thermochemical Water Splitting Cycle. *Proc. Natl. Acad. Sci. U.S.A.* **2012**, *109*, 9260−9264.

(8) Escande, V.; Lam, C. H.; Coish, P.; Anastas, P. T. Heterogeneous Sodium-Manganese Oxide Catalyzed Aerobic Oxidative Cleavage of 1,2-Diols. *Angew. Chem., Int. Ed.* **2017**, *56*, 9561−9565.

(9) Jia, X.; Ma, J.; Wang, M.; Li, X.; Gao, J.; Xu, J. Alkali $\alpha$-$MnO_2$/$Na_xMnO_2$ Collaboratively Catalyzed Ammoxidation−Pinner Tandem Reaction of Aldehydes. *Catal. Sci. Technol.* **2016**, *6*, 7429−7436.

(10) Bevara, S.; Giri, P.; Achary, S. N.; Bhallerao, G.; Mishra, R. K.; Kumar, A.; Kaushik, C. P.; Tyagi, A. K. Synthetic Na/K-Birnessite for Efficient Management of Sr(II) from Nuclear Waste. *J. Environ. Chem. Eng.* **2018**, *6*, 7200−7213.

(11) Chakravarty, R.; Bevara, S.; Bahadur, J.; Chakraborty, S.; Dev Sarma, H.; Achary, S. N.; Dash, A.; Tyagi, A. K. Birnessite: A New-Generation and Cost Effective Ion Exchange Material for Separation of Clinical-Grade $^{90}$Y from $^{90}$Sr/ $^{90}$Y Mixture. *ChemistrySelect* **2018**, *3*, 10670−10676.

(12) Guidotti, T. L. Hydrogen Sulfide: Advances in Understanding Human Toxicity. *Int. J. Toxicol.* **2010**, *29*, 569−581.

(13) Martínez-Ahumada, E.; Díaz-Ramírez, M. L.; Velásquez-Hernández, M.; Jancik, V.; Ibarra, I. A. Capture of Toxic Gases in MOFs: $SO_2$, $H_2S$, $NH_3$ and $NO_x$. *Chem. Sci.* **2021**, *12*, 6772−6799.

(14) Fuller, R.; Landrigan, P. J.; Balakrishnan, K.; Bathan, G.; Bose-O'Reilly, S.; Brauer, M.; Caravanos, J.; Chiles, T.; Cohen, A.; Corra, L.; Cropper, M.; Ferraro, G.; Hanna, J.; Hanrahan, D.; Hu, H.; Hunter, D.; Janata, G.; Kupka, R.; Lanphear, B.; Lichtveld, M.; Martin, K.; Mustapha, A.; Sanchez-Triana, E.; Sandilya, K.; Schaefli, L.; Shaw, J.; Seddon, J.; Suk, W.; Téllez-Rojo, M. M.; Yan, C. Pollution and Health: A Progress Update. *Lancet Planet. Health* **2022**, *6*, e535−e547.

(15) Manisalidis, I.; Stavropoulou, E.; Stavropoulos, A.; Bezirtzoglou, E. Environmental and Health Impacts of Air Pollution: A Review. *Front. Public Health* **2020**, *8*, 14.

(16) Shah, M. S.; Tsapatsis, M.; Siepmann, J. I. Hydrogen Sulfide Capture: From Absorption in Polar Liquids to Oxide, Zeolite, and Metal−Organic Framework Adsorbents and Membranes. *Chem. Rev.* **2017**, *117*, 9755−9803.

(17) Rezaei, F.; Rownaghi, A. A.; Monjezi, S.; Lively, R. P.; Jones, C. W. $SO_x/NO_x$ Removal from Flue Gas Streams by Solid Adsorbents: A Review of Current Challenges and Future Directions. *Energy Fuels* **2015**, *29*, 5467−5486.

(18) Liu, S.; Fan, C.-Z.; Zhang, Y.; Li, C.-H.; You, X.-Z. Low-Temperature Synthesis of $Na_2Mn_5O_{10}$ for Supercapacitor Applications. *J. Power Sources* **2011**, *196*, 10502−10506.

(19) Song, B.; Tang, M.; Hu, E.; Borkiewicz, O. J.; Wiaderek, K. M.; Zhang, Y.; Phillip, N. D.; Liu, X.; Shadike, Z.; Li, C.; Song, L.; Hu, Y.-Y.; Chi, M.; Veith, G. M.; Yang, X.-Q.; Liu, J.; Nanda, J.; Page, K.; Huq, A. Understanding the Low-Voltage Hysteresis of Anionic Redox in $Na_2Mn_3O_7$. *Chem. Mater.* **2019**, *31*, 3756−3765.

(20) Jarosch, D. Crystal Structure Refinement and Reflectance Measurements of Hausmannite, $Mn_3O_4$. *Mineral. Petrol.* **1987**, *37*, 15−23.

(21) Sehrawat, D.; Rawal, A.; Cheong, S.; Avdeev, M.; Ling, C. D.; Kimpton, J. A.; Sharma, N. Alkali Metal-Modified P2 $Na_xMnO_2$: Crystal Structure and Application in Sodium-Ion Batteries. *Inorg. Chem.* **2020**, *59*, 12143−12155.

(22) Thommes, M.; Kaneko, K.; Neimark, A. V.; Olivier, J. P.; Rodriguez-Reinoso, F.; Rouquerol, J.; Sing, K. S. W. Physisorption of Gases, with Special Reference to the Evaluation of Surface Area and Pore Size Distribution (IUPAC Technical Report). *Pure Appl. Chem.* **2015**, *87*, 1051−1069.

(23) Gupta, N. K.; Bae, J.; Kim, K. S. From MOF-199 Microrods to CuO Nanoparticles for Room-Temperature Desulfurization: Regeneration and Repurposing Spent Adsorbents as Sustainable Approaches. *ACS Omega* **2021**, *6*, 25631−25641.

(24) Zhang, Y.; Liu, Z.; Deng, H.; Xie, J.; Xia, J.; Nie, S.; Liu, W.; Liu, L.; Wang, X. Rectangular Tunnel-Structured $Na_{0.4}MnO_2$ as a Promising Cathode Material Withstanding a High Cutoff Voltage for Na-Ion Batteries. *ChemElectroChem* **2019**, *6*, 1711−1721.

(25) Zeng, F.; Pan, Y.; Yang, Y.; Li, Q.; Li, G.; Hou, Z.; Gu, G. Facile Construction of $Mn_3O_4$-$MnO_2$ Hetero-Nanorods/Graphene Nanocomposite for Highly Sensitive Electrochemical Detection of Hydrogen Peroxide. *Electrochim. Acta* **2016**, *196*, 587−596.

(26) Hakim, C.; Ma, L. A.; Duda, L. C.; Younesi, R.; Brandell, D.; Edström, K.; Saadoune, I. Anionic Redox and Electrochemical Kinetics of the $Na_2Mn_3O_7$ Cathode Material for Sodium-Ion Batteries. *Energy Fuels* **2022**, *36*, 4015−4025.

(27) Chae, M. S.; Chakraborty, A.; Kunnikuruvan, S.; Attias, R.; Maddukuri, S.; Gofer, Y.; Major, D. T.; Aurbach, D. Vacancy-Driven High Rate Capabilities in Calcium-Doped $Na_{0.4}MnO_2$ Cathodes for Aqueous Sodium-Ion Batteries. *Adv. Energy Mater.* **2020**, *10*, No. 2002077.

(28) Gupta, N. K.; Bae, J.; Kim, K. S. Metal-Organic Framework-Derived $NaMn_xO_y$ Hexagonal Microsheets for Superior Adsorptive-Oxidative Removal of Hydrogen Sulfide in Ambient Conditions. *Chem. Eng. J.* **2021**, No. 130909.

(29) Ilton, E. S.; Post, J. E.; Heaney, P. J.; Ling, F. T.; Kerisit, S. N. XPS Determination of Mn Oxidation States in Mn (Hydr)Oxides. *Appl. Surf. Sci.* **2016**, *366*, 475−485.

(30) Wu, T.-H.; Hesp, D.; Dhanak, V.; Collins, C.; Braga, F.; Hardwick, L. J.; Hu, C.-C. Charge Storage Mechanism of Activated Manganese Oxide Composites for Pseudocapacitors. *J. Mater. Chem. A* **2015**, *3*, 12786−12795.

(31) Bradley, S. J.; Kroon, R.; Laufersky, G.; Röding, M.; Goreham, R. V.; Gschneidtner, T.; Schroeder, K.; Moth-Poulsen, K.; Andersson, M.; Nann, T. Heterogeneity in the Fluorescence of Graphene and Graphene Oxide Quantum Dots. *Microchim. Acta* **2017**, *184*, 871−878.

(32) Zhao, Y.; Zhang, Z.; Yang, C.; Fan, H.; Wang, J.; Tian, Z.; Zhang, H. Critical Role of Water on the Surface of ZnO in $H_2S$ Removal at Room Temperature. *Ind. Eng. Chem. Res.* **2018**, *57*, 15366−15374.

(33) Long, J. W.; Wallace, J. M.; Peterson, G. W.; Huynh, K. Manganese Oxide Nanoarchitectures as Broad-Spectrum Sorbents for Toxic Gases. *ACS Appl. Mater. Interfaces* **2016**, *8*, 1184−1193.

(34) Xue, M.; Chitrakar, R.; Sakane, K.; Ooi, K. Screening of Adsorbents for Removal of $H_2S$ at Room Temperature. *Green Chem.* **2003**, *5*, 529−534.

(35) Bagreev, A.; Rahman, H.; Bandosz, T. J. Thermal Regeneration of a Spent Activated Carbon Previously Used as Hydrogen Sulfide Adsorbent. *Carbon* **2001**, *39*, 1319−1326.

(36) Seredych, M.; Bandosz, T. J. Reactive Adsorption of Hydrogen Sulfide on Graphite Oxide/$Zr(OH)_4$ Composites. *Chem. Eng. J.* **2011**, *166*, 1032−1038.

(37) Yang, W.; Zhang, J.; Ma, Q.; Zhao, Y.; Liu, Y.; He, H. Heterogeneous Reaction of $SO_2$ on Manganese Oxides: The Effect of Crystal Structure and Relative Humidity. *Sci. Rep.* **2017**, *7*, No. 4550.

(38) Marinova, D.; Kostov, V.; Nikolova, R.; Kukeva, R.; Zhecheva, E.; Sendova-Vasileva, M.; Stoyanova, R. From Kröhnkite- to Alluaudite-Type of Structure: Novel Method of Synthesis of Sodium Manganese Sulfates with Electrochemical Properties in Alkali-Metal Ion Batteries. *J. Mater. Chem. A* **2015**, *3*, 22287−22299.

(39) Toupin, M.; Brousse, T.; Bélanger, D. Charge Storage Mechanism of $MnO_2$ Electrode Used in Aqueous Electrochemical Capacitor. *Chem. Mater.* **2004**, *16*, 3184−3190.

(40) Gupta, N. K.; Bae, J.; Kim, K. S. Metal Organic Framework Derived $NaCo_xO_y$ for Room Temperature Hydrogen Sulfide Removal. *Sci. Rep.* **2021**, *11*, No. 14740.

(41) Wang, J.; Yang, C.; Zhao, Y.-R.; Fan, H.-L.; Wang, Z.-D.; Shangguan, J.; Mi, J. Synthesis of Porous Cobalt Oxide and Its Performance for $H_2S$ Removal at Room Temperature. *Ind. Eng. Chem. Res.* **2017**, *56*, 12621−12629.

(42) Song, H. S.; Park, M. G.; Kwon, S. J.; Yi, K. B.; Croiset, E.; Chen, Z.; Nam, S. C. Hydrogen Sulfide Adsorption on Nano-Sized Zinc Oxide/Reduced Graphite Oxide Composite at Ambient Condition. *Appl. Surf. Sci.* **2013**, *276*, 646−652.

(43) Quesne-Turin, A.; Flahaut, D.; Croguennec, L.; Vallverdu, G.; Allouche, J.; Charles-Blin, Y.; Chotard, J.-N.; Ménétrier, M.; Baraille, I. Surface Reactivity of $Li_2MnO_3$: First-Principles and Experimental Study. *ACS Appl. Mater. Interfaces* **2017**, *9*, 44222−44230.

(44) Quesne-Turin, A.; Flahaut, D.; Salvato Vallverdu, G.; Croguennec, L.; Allouche, J.; Weill, F.; Ménétrier, M.; Baraille, I. Surface Reactivity of $Li_2MnO_3$: Structural and Morphological Impact. *Appl. Surf. Sci.* **2021**, *542*, No. 148514.

(45) Nanayakkara, C. E.; Pettibone, J.; Grassian, V. H. Sulfur Dioxide Adsorption and Photooxidation on Isotopically-Labeled Titanium Dioxide Nanoparticle Surfaces: Roles of Surface Hydroxyl Groups and Adsorbed Water in the Formation and Stability of Adsorbed Sulfite and Sulfate. *Phys. Chem. Chem. Phys.* **2012**, *14*, 6957.

(46) Cant, D. J. H.; Syres, K. L.; Lunt, P. J. B.; Radtke, H.; Treacy, J.; Thomas, P. J.; Lewis, E. A.; Haigh, S. J.; O'Brien, P.; Schulte, K.; Bondino, F.; Magnano, E.; Flavell, W. R. Surface Properties of Nanocrystalline PbS Films Deposited at the Water−Oil Interface: A Study of Atmospheric Aging. *Langmuir* **2015**, *31*, 1445−1453.